

In vitro reconstitution and crystal structure of *p*-aminobenzoate *N*-oxygenase (AurF) involved in aureothin biosynthesis

Yoo Seong Choi*, Houjin Zhang^{†‡}, Joseph S. Brunzelle[§], Satish K. Nair^{††¶||}, and Huimin Zhao^{**†¶||**}

Departments of *Chemical and Biomolecular Engineering, [†]Biochemistry, and [¶]Chemistry, **Center for Biophysics and Computational Biology, and [‡]Institute for Genomic Biology, University of Illinois at Urbana–Champaign, 600 South Mathews Avenue, Urbana, IL 61801; and [§]Life Sciences Collaborative Access Team, Argonne National Laboratories, Argonne, IL 60439

Edited by Brian W. Matthews, University of Oregon, Eugene, OR, and approved March 18, 2008 (received for review December 21, 2007)

p-aminobenzoate *N*-oxygenase (AurF) from *Streptomyces thioluteus* catalyzes the formation of unusual polyketide synthase starter unit *p*-nitrobenzoic acid (pNBA) from *p*-aminobenzoic acid (pABA) in the biosynthesis of antibiotic aureothin. AurF is a metalloenzyme, but its native enzymatic activity has not been demonstrated *in vitro*, and its catalytic mechanism is unclear. In addition, the nature of the cofactor remains a controversy. Here, we report the *in vitro* reconstitution of the AurF enzyme activity, the crystal structure of AurF in the oxidized state, and the cocrystal structure of AurF with its product pNBA. Our combined biochemical and structural analysis unequivocally indicates that AurF is a non-heme di-iron monooxygenase that catalyzes sequential oxidation of aminoarenes to nitroarenes via hydroxylamine and nitroso intermediates.

di-iron enzymes | metalloenzymes | *N*-oxygenation | reaction mechanism

Aromatic nitro groups are relatively rare functional groups in natural products but are found in diverse types of important antibiotics, such as chloramphenicol, pyrrolnitrin, aureothin, azomycin, and rufomycin (1–3). The biosynthesis of aromatic nitro groups is poorly understood. To date, only two enzymes have been shown to catalyze the oxidation of an arylamine group to an aryl nitro group. One is *p*-nitrobenzoate *N*-oxygenase (AurF) involved in the biosynthesis of aureothin (4). The other, aminopyrrolnitrin *N*-oxygenase (PrnD), a Rieske mononuclear non-heme iron enzyme involved in the biosynthesis of pyrrolnitrin, catalyzes the conversion of aminopyrrolnitrin to pyrrolnitrin (3, 5). Notably, AurF shares no sequence homology with any other functionally characterized oxygenases in the Swiss-Prot database, and the purified enzyme did not show any native enzymatic activity (6, 7), although a “peroxide shunt” was recently found to be able to restore the enzymatic activity (8).

We previously cloned *aurF* from *Streptomyces thioluteus* [American Type Culture Collection (ATCC) accession number 12310] and developed a high-level heterologous expression system in *Escherichia coli*. A combination of experimental results from bioinformatics, inductively coupled plasma (ICP) mass spectrometry (MS), and electron paramagnetic resonance (EPR) suggested that AurF is a di-iron enzyme (6). In sharp contrast, Hertweck and coworkers recently concluded that AurF is a di-manganese enzyme on the basis of ICP-MS data of a maltose binding protein-AurF fusion protein (8), crystal structure of AurF in an oxidized state and anomalous x-ray diffraction (9), and structure-based site-directed mutagenesis (7). As an attempt to reconcile the apparently contradictory results between the two studies, Bollinger and coworkers proposed that AurF may contain a heterodinuclear Mn/Fe cofactor (10), similar to the R2 subunit of class Ic ribonucleotide reductase from *Chlamydia trachomatis* (11).

Because of the unknown nature of the cofactor and, more importantly, the inability to obtain catalytically active AurF enzyme *in vitro*, the catalytic mechanism of AurF remains

unclear. It was proposed that three successive two-electron oxidations produce *p*-hydroxylaminobenzoate (pHABA), *p*-nitrosobenzoate, and finally the *p*-nitrobenzoic acid (pNBA) product (2, 6). The hydroxylamine intermediate was demonstrated; however, the nitroso intermediate has not been detected. In addition, many fundamental questions about the enzymology of AurF, such as di-oxygen activation, electron transfer, substrate binding, and product release remain to be addressed.

Here, we report the first successful *in vitro* reconstitution of the native enzymatic activity of AurF, using both chemical reductants and biological reductants. In addition, we report the crystal structure of AurF in the oxidized state and the cocrystal structure of AurF with its product pNBA. The combined biochemical and structural analysis clearly indicates that AurF is a di-iron enzyme that catalyzes stepwise *N*-monooxygenation. This work has laid out a solid foundation for further investigation of the catalytic mechanisms of AurF, including the di-oxygen activation and electron transfer pathways and protein engineering of AurF for biotechnological applications.

Results and Discussion

***In Vitro* Reconstitution of AurF Enzymatic Activity, Using Chemical Reductants.** To resolve the controversy on the nature of the cofactor in AurF and further investigate the catalytic mechanism of AurF, we sought to reconstitute the native enzymatic activity of AurF *in vitro*. Because most known di-iron enzymes are catalytically active in a reduced (diferrous) form (12, 13), we first used chemical reductants to prepare diferrous AurF for single-turnover experiments. Based on the protocols of similar experiments developed for the hydroxylase subunit of the soluble methane monooxygenase (MMOH) (14, 15), we used either sodium dithionite or ascorbate as a chemical reductant and various chemicals, including phenazine methosulfate (PMS), methyl viologen, and proflavin as an electron mediator. It was found that the *in vitro* enzymatic activity of AurF was best reconstituted in the presence of PMS and ascorbate [supporting information (SI) Fig. S1]. The reduced AurF generated an EPR signal at $g = 16$ at $T = 4$ K with the magnetic microwave field

Author contributions: Y.S.C., S.K.N., and H. Zhao designed research; Y.S.C., H. Zhang, and J.S.B. performed research; Y.S.C., S.K.N., and H. Zhao analyzed data; and Y.S.C., S.K.N., and H. Zhao wrote the paper.

The authors declare no conflict of interest.

This article is a PNAS Direct Submission.

Freely available online through the PNAS open access option.

Data deposition: The coordinates and structure factors have been deposited in the Protein Data Bank, www.pdb.org [ID codes 3CHU (AurF-orthorhombic crystal form), 3CHI (AurF-monoclinic form), and 3CHT (AurF-pNBA complex)].

¶To whom correspondence may be addressed. E-mail: snair@uiuc.edu or zhao5@uiuc.edu.

This article contains supporting information online at www.pnas.org/cgi/content/full/0712073105/DCSupplemental.

© 2008 by The National Academy of Sciences of the USA

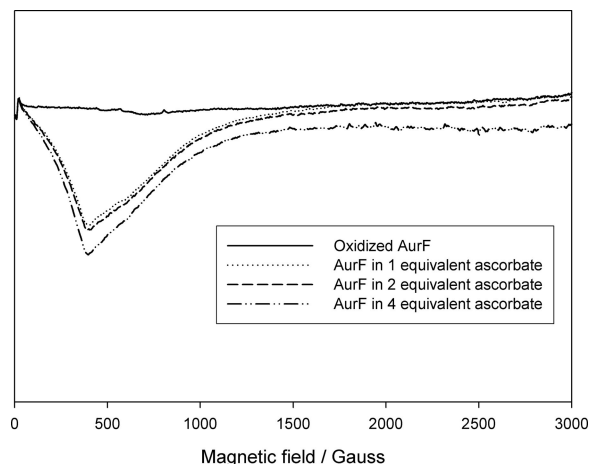


Fig. 1. X-band EPR spectra of the fully reduced AurF at 4 K, using microwave B_1 parallel to the static field B .

B_1 applied parallel to the static field B , which is similar to that observed for MMOH (16), toluene-4-monooxygenase (17), and phenol hydroxylase (18). The $g = 16$ EPR signal is characteristic of the ferromagnetically coupled diferrous state (13). The intensity of the signal increased as the concentration of ascorbate was raised (Fig. 1). Of note, the mixed valent AurF generated an EPR spectrum showing g_x , g_y , and g_z values of 1.94, 1.79, and 1.70, respectively, in normal mode, also indicative of the mixed-valent di-iron state (6). No turnover after addition of an O_2 -free solution containing pABA was observed, whereas the exposure of O_2 activated AurF. The yield of the final product pNBA was $37.2 \pm 4.2\%$ when equimoles of PMS and pABA and 4 eq of ascorbate were used.

Determination of the Iron-to-Enzyme Ratio in AurF. The iron-to-enzyme ratio of purified AurF was determined to be 2.2 by using ICP-MS analysis (6) and a colorimetric assay based on the ferriox chelator (19). The protein with a Mn-free di-iron center gave maximal activity and the gradual decrease of iron content in AurF led to the gradual decrease of *in vitro* enzymatic activity (Table 1). Contrary to the finding by the Hertweck group that “manganese was enriched by a factor of ≈ 20 in relation to iron” in purified AurF proteins (8, 9), our data clearly show a high selectivity of the protein for iron (rows 3 and 4 in Table 1). This discrepancy is likely due to the use of Fe(III) citrate hydrate and unusually high concentrations of iron and manganese in the culture media in the previous study rather than $Fe(NH_4)_2(SO_4)_2$, which was used in our experiments and many other similar studies involving di-iron enzymes. Note that iron and manganese are accumulated by *E. coli* cells via different active transport systems (20, 21), and it is conceivable that AurF may not be capable of incorporating Fe(III) during protein expression and folding. Also note that we could not obtain the apo-form of AurF by using various

metal-chelating reagents (data not shown), and, therefore, no *in vitro* metal titration experiments were performed.

In Vitro Reconstitution of AurF Enzymatic Activity, Using Biological Reductants. In addition to the above chemical reduction method, we used a biological reduction method to prepare reduced AurF enzymes. Thorough examination of the aureothin biosynthesis gene cluster failed to identify a reductase or similar electron transfer proteins that may transfer electrons to AurF. However, AurF is a homodimer based on size exclusion HPLC (Fig. S2), which is similar to the castor stearyl acyl carrier protein Δ^9 desaturase (Δ^9D) but dissimilar to soluble methane monooxygenase (MMO) and ribonucleotide reductase. In the MMO system, a reductase (MMOR) transfers the electrons from NADH to MMOH (22), whereas, in the Δ^9D system, two proteins, NADPH:ferredoxin oxidoreductase (FdR) and [2Fe-2S] ferredoxin (Fd), constitute an electron transfer chain between NAD(P)H and Δ^9D (13). The electron transfer chain for the ribonucleotide reductase is still controversial (13). In addition, heterologous expression of AurF in both *Streptomyces lividans* and *E. coli* yielded biologically active AurF in whole cells (6), suggesting some generic electron transfer proteins and reducing equivalents could reconstitute the *in vivo* and possibly *in vitro* activity of AurF. Thus, we followed the Δ^9D system and found that the enzymatic activity of the oxidized AurF was fully reconstituted in the presence of a surrogate FdR and a surrogate Fd from *Anabaena* sp. PCC 7119, and NADPH.

The steady-state kinetic parameters of AurF were determined by using pABA as a substrate. AurF had $k_{cat} = 6.21 \pm 0.52 \text{ min}^{-1}$, $K_m = 5.24 \pm 0.64 \mu\text{M}$, and $k_{cat}/K_m = 1.21 \pm 0.31 \text{ min}^{-1}\mu\text{M}^{-1}$ at 20°C . Notably, multiple turnovers were also observed in an NADH/PMS system, similar to cytochrome P450_{CAM} (23). The corresponding kinetic parameters were $k_{cat} = 5.04 \pm 0.22 \text{ min}^{-1}$, $K_m = 8.89 \pm 0.87 \mu\text{M}$, and $k_{cat}/K_m = 0.57 \pm 0.03 \text{ min}^{-1}\mu\text{M}^{-1}$ at 20°C . These two sets of kinetic data are consistent with each other. Note that the specific activity of di-manganese-AurF, using the peroxide shunt based enzymatic activity assay [0.0032 units/mg (AurF) at 23°C (9)], is ≈ 2 –2.5% of our observed activity [0.13–0.16 units/mg (AurF)], which is consistent with the specific activity of AurF containing 1.94 Mn and 0.11 Fe per monomer (row 5 in Table 1, a form similar to the AurF enzyme reported by the Hertweck group). This indicates that the enzymatic activity detected in the di-manganese AurF protein most likely originated from the small amount of the di-iron AurF in the protein sample.

Determination of the Crystal Structure of AurF in the Oxidized State.

To further validate the nature of the cofactor and better understand the catalytic mechanism, we sought to determine the crystal structures of AurF with and without pABA or pNBA. Crystals of purified AurF enzymes were grown under both aerobic and anaerobic conditions. Orthorhombic crystals grown aerobically (oxidized AurF) were used for initial phase determination, and the 2.2 Å resolution structure has been determined by single-wavelength anomalous diffraction methods,

Table 1. Dependence of the catalytic activity of AurF isolated from minimal medium culture with different Fe:Mn ratio

Fe:Mn ratio in minimal medium (final total concentration, 1 mM)	Fe content per protein monomer	Mn content per protein monomer	Relative activity, %
Fe:Mn = 1:0 (Fe only)	2.22 ± 0.16	0	100 ± 8.2
Fe:Mn = 0.75:0.25	1.98 ± 0.07	0.61	87.5 ± 5.9
Fe:Mn = 0.5:0.5	1.89 ± 0.26	0.18	79.8 ± 2.1
Fe:Mn = 0.25:0.75	1.77 ± 0.05	0.80	70.6 ± 4.0
Fe:Mn = 0:1 (Mn only)	0.11 ± 0.07	1.94	5.8 ± 1.0

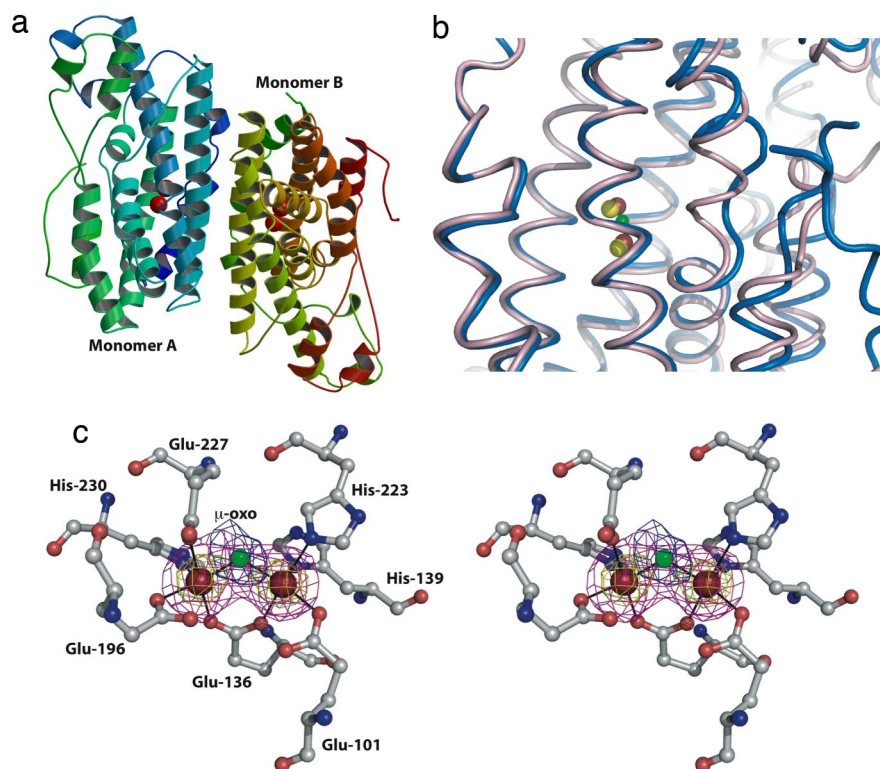


Fig. 2. Structural analysis of AurF. (a) Overall view of the di-iron AurF homodimer shown in a ribbon representation with a color ramp of blue to red (amino to carboxyl terminus). The iron atoms are shown as red spheres. (b) A diagram representation of the superposition of di-iron AurF (shown in blue tube) and di-manganese AurF (shown in pink tube) near the active site. The iron atoms are shown as red spheres, the bridging μ -oxo atom is shown as a green sphere, and the manganese atoms are shown in yellow. (c) Stereoview of the active site of unliganded AurF illustrating the protein ligands to the metal. The iron atoms are shown as dark-red spheres, and the bridging μ -oxo species is shown as a green sphere. Two difference Fourier electron density maps calculated with coefficients $|F_{\text{obs}}| - |F_{\text{calc}}|$ are superimposed on the coordinates. The first map is calculated with phases from the refined model of unliganded AurF minus the two iron atoms and the μ -oxo bridge and is contoured at 3 (colored in magenta) and 11 (colored in yellow) standard deviations above background (σ). The second difference Fourier map was calculated in a similar fashion, but only the bridging μ -oxo atom was omitted before calculations and this map is contoured at 4 σ (blue).

using a single mercury derivative (Table S1). The overall structure is composed nearly entirely of α -helices (Fig. 2a). As in solution, the molecule is a homodimer in the crystal and the intersubunit interface consists of a helical bundle (nearly 2,100 \AA^2 of buried surface area within the dimer). The electron density of the polypeptide chain is nearly continuous throughout the structure with the exception of the amino terminal 23 residues, the carboxyl-terminal 6 residues, and residues in a linker between amino acids 291 and 299. Despite the lack of appreciable sequence similarity, the overall fold of AurF is reminiscent to that of other di-iron oxygenase, such as MMOH (22), the R2 subunit of *E. coli* ribonucleotide reductase (24), and $\Delta^9\text{D}$ (25).

Consistent with our biochemical and biophysical results, strong electron density, corresponding to the di-iron center, can be observed within the four-helix core of AurF. As shown in Fig. 2c, protein residues Glu-101, Glu-136, His-139, Glu-196, His-223, Glu-227, and His-230 engage the two iron ions. The distances between the two iron atoms are 3.43 \AA for monomer A and 3.45 \AA for monomer B. Additionally, clear and convincing density can be observed for the μ -oxo bridge at each of the two active sites, with distances that range from 1.85 to 2.02 \AA , consistent with the range of values observed at the (μ -oxo)bis(μ -carboxylato)diiron(III) centers in other di-iron oxygenases (13). To further confirm the identity of the metal ligand at the active site of the crystallized species, we calculated anomalous difference Fourier maps, using phases from the final model (minus all metal atoms) and coefficients from Bijvoet differences from data collected from a single crystal near the iron and manganese absorption edges, respectively. These maps show significant

spherical density (>10 standard deviations above noise) at the two metals with Bijvoet difference data collected near the iron absorption edge but only weak spurious density (<4 standard deviations above noise) at one of the metals from Bijvoet difference data near the manganese edge (Fig. 3). These data are consistent with our approximation of an iron to manganese ratio of at least 20:1 in these crystals.

Determination of the Cocrystal Structure of AurF with Its Product pNBA. To obtain crystals of the AurF-substrate or product complex, crystals of the unliganded enzyme were grown under anaerobic conditions, using a glove box apparatus. Cocrystals of the binary complex grown under anaerobic conditions did not show any observable features in experimental electron density maps corresponding to the ligand. Because there were no significant differences in the active site structure of anaerobically produced crystals of AurF, these were not further pursued for structural studies. Because our biochemical studies demonstrate that binding of molecular oxygen must occur before ligand binding (data not shown), crystals grown anaerobically were moved to an aerobic environment and soaked with a solution containing either 5 mM substrate pABA or 5 mM product pNBA in the presence of a chemical reductant (1 mM sodium ascorbate). Weak but notable density can be observed in the active site of one monomer corresponding to the product pNBA (average B-factor of 64 for the ligand versus 42 for the protein). The ligand was modeled into these features (Fig. 4), providing a model for the ternary complex (AurF, μ -oxo bridge, pNBA). Because we cannot distinguish between nitrogen and oxygen atoms at the

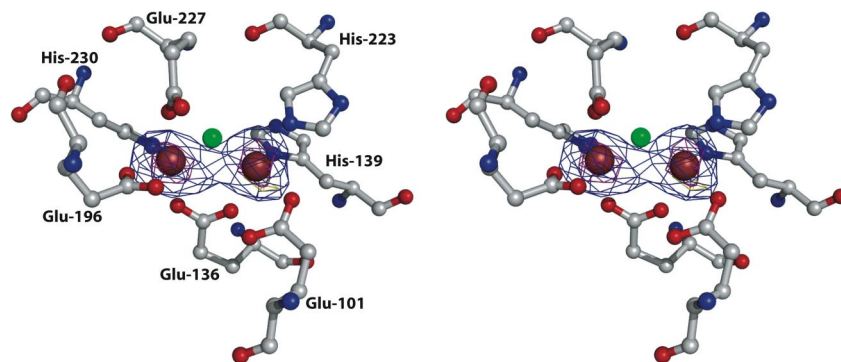


Fig. 3. Stereoview of anomalous difference Fourier electron density maps calculated with phases from the final refined model of AurF minus the two metal atoms and coefficients $|F^+| - |F^-|$, corresponding to wavelength dependent Bijvoet differences. Maps calculated from data collected at the iron absorption edge ($\lambda = 1.7220 \text{ \AA}$) are shown in blue (6σ) and magenta (11σ), and maps calculated from data collected at the absorption edge for manganese ($\lambda = 1.8785 \text{ \AA}$) are shown in yellow (4σ). The final refined coordinates are superimposed on the maps. The two iron μ -oxo atoms are shown as dark-red spheres, and the bridging μ -oxo atom is shown as a green sphere.

resolution of our structures, it is possible that the product could be bound with the nitroso group pointing away from the metal and the carboxylate pointing toward the di-iron center. In this instance, Glu-196 would be protonated to accommodate the carboxylate-carboxylic acid interaction. This unproductive mode of binding cannot be formally ruled out based on our data.

The aromatic ligand is bound near a hydrophobic cavity adjacent to the di-iron center formed by residues Tyr-93, Val-97, Thr-100, Ile-199, and Leu-203. The carboxylate of the product is stabilized at the active site by hydrogen bond interactions with Tyr-93, and Asn-200. The nitro group of the product coordinates with one of the iron atoms, and form a hydrogen bond with metal-ligand Glu-196, which undergoes a slight conformational shift as a result. Additional favorable electrostatic interactions occur with the guanidinium group of Arg-302, which also reorients, relative to the unliganded structure, to face into the active site (Fig. 4).

Structural Comparisons Between the Di-Iron AurF and the Di-Manganese AurF. During the preparation of this article, the Schulz and coworkers (9) reported that the structure of manganese substituted AurF from protein samples cultivated under high concentrations of this divalent metal. Although this structure unequivocally demonstrates a di-manganese center, there are significant notable differences in the active site architecture compared with

our structure of di-iron AurF (Figs. 2*b* and 5). Specifically, a stretch of residues encompassing Ala-195 through Asn-200 is shifted toward the di-metal center resulting in the movement of Ile-199 into the active site (Fig. 5*a* and *c*). Additionally, Arg-96, Leu-202, Leu-203, and Phe-264 are also displaced toward the metal center to form a collapsed, shallow active site (Fig. 5*b* and *c*). A structure based alignment of the alpha carbons of di-iron AurF with di-manganese AurF results in a root mean square deviation of 2.1 \AA over 590 superimposed $C\alpha$ of the dimer. A comparison of the individual subunits yields a root mean square deviation of 1.6 \AA over 295 superimposed $C\alpha$ atoms and 1.6 \AA over 1180 superimposed peptide atoms. We note that the active site architecture observed in our structure of the di-iron AurF is conserved between two different crystal forms (Table S1), ruling out crystal packing artifacts as a source for these differences.

The conformation of these residues in the reported structure of di-manganese AurF would result in steric interference with the binding of pABA at the active site location identified in our cocrystal structure. Additionally, in this earlier report, modeling of substrate pABA into the active site of manganese AurF required significant conformational alterations of the side chains of Arg-96, Leu-202, and Phe-264 (9). Hence, substitution of manganese at the di-metal center would most likely result in an inactive enzyme, consistent with our biochemical observations. Finally, we note that conformation of the metal coordinating residue Glu-227 in the manganese substituted AurF structure is also different from that observed in our structure of the di-iron enzyme. In the inactive manganese AurF structure (9), the carboxylate side chain of Glu-227 is located at a position occupied by the μ -oxo bridge in our structure of di-iron AurF.

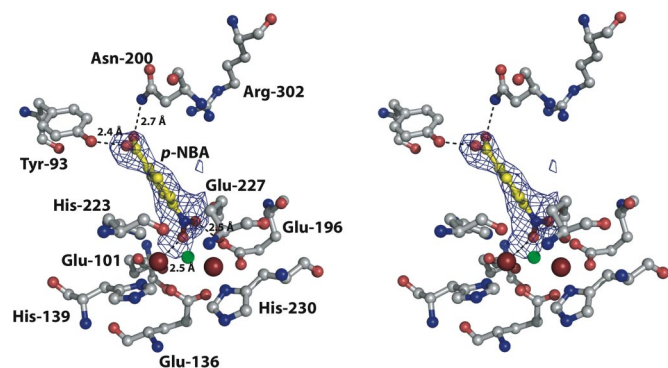


Fig. 4. Stereoview of difference Fourier electron density maps calculated with coefficients $|F_{\text{obs}}| - |F_{\text{calc}}|$ and phases from the refined model of the AurF-product complex minus the atoms of the partially occupied molecule of pNBA, contoured at 2.3σ over background. The final refined coordinates of the complex are superimposed. The two iron atoms are shown as dark-red spheres, the bridging μ -oxo atom is shown as a green sphere, and the atoms of the ligand are shown in yellow.

Detection of the Elusive Nitroso Intermediate. The catalytic mechanism of AurF was first proposed by the Hertweck group on the basis of *in vivo* assay data (2). In this mechanism (Scheme S1*a*), the first step involves the addition of an oxygen atom to produce pHABA from pABA. The later steps involve the addition of another oxygen atom, followed by a dehydration step to a nitroso compound, and subsequently the addition of a third oxygen atom to produce the nitro compound. Recently, based on HPLC analysis and $^{18}\text{O}_2$ labeling studies, we proposed a revised mechanism (Scheme S1*b*), in which pHABA is directly converted into a nitroso compound by dehydrogenation (6). However, in both mechanisms, the nitroso compound was not detected. With the availability of *in vitro* reconstituted AurF, the elusive nitroso compound was experimentally isolated (Fig. 6), demonstrating that AurF catalyzes sequential oxidation of pABA to pNBA via hydroxylamine and nitroso intermediates.

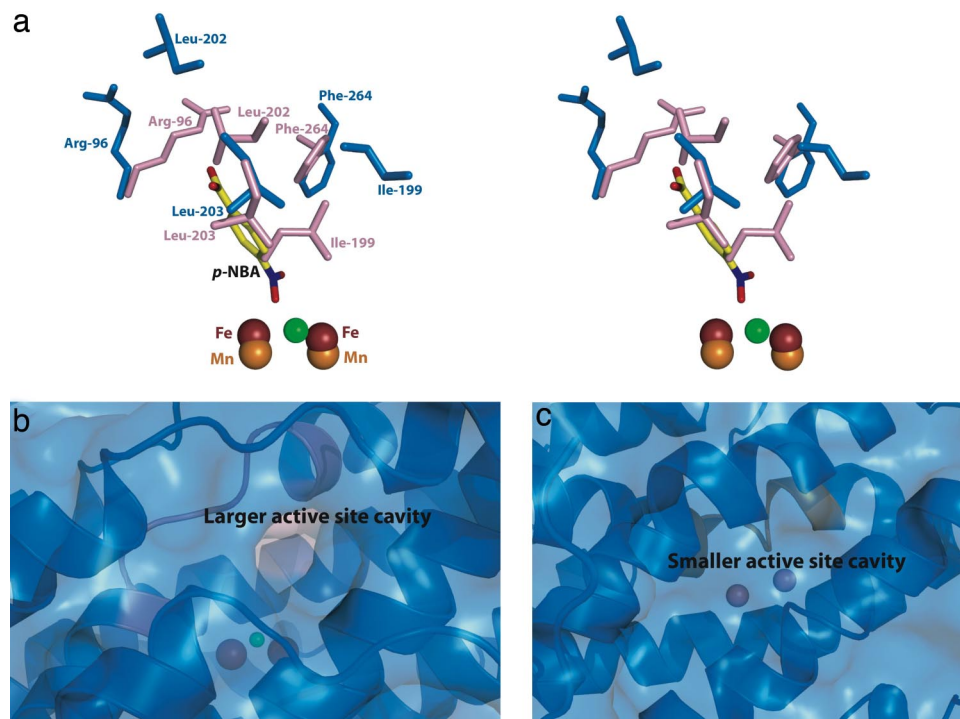


Fig. 5. Structural comparisons. (a) Comparison of the crystal structures of di-iron AurF (in blue) and di-manganese AurF (in pink) (9). The positions of protein residues Arg-96, Ile-199, Leu-202, Leu-203, and Phe-264 vary considerably between the two structures, and these residues are compressed into the active site in the structure of di-manganese AurF. (b and c) The active site of the di-iron AurF contains a well formed cavity that allows for the binding of substrate without significant changes in the protein scaffold, whereas the active site of di-manganese AurF contains a much smaller cavity and would require rearrangement of residues to accommodate the substrate.

In conclusion, we have clearly shown that AurF is a di-iron enzyme that catalyzes unusual sequential N-oxygenation. The architecture of the di-iron center and unique chemistry of AurF and ease of protein preparation and crystallization make AurF an excellent model for further investigation of the molecular mechanism of di-oxygen activation. In addition, the crystal structure of AurF should aid protein engineering of AurF with altered or novel substrate specificity and novel chemistry for combinatorial biosynthesis and industrial biocatalysis.

Materials and Methods

Overexpression and Purification of AurF, [2Fe-2S] Ferredoxin, and Ferredoxin-NADP⁺ Reductase. To prepare AurF with different iron/manganese ratios, *E. coli* cells harboring the AurF encoding plasmid (6) were grown in minimal media [M9, 12.8 g/liter Na₂HPO₄·7H₂O, 3 g/liter KH₂PO₄, 1 g/liter NH₄Cl, 0.5 g/liter NaCl, 2 mM MgSO₄, 0.4% (vol/vol) glucose, 0.1 mM CaCl₂, and 1 mg/liter thiamine] at 37°C at 250 rpm until OD₆₀₀ of 0.8 was reached. Then, the culture media was supplemented with 100 mg/liter each of L-lysine, L-threonine, L-phenylalanine, 50 mg/liter each of L-leucine, L-isoleucine, L-valine, 60 mg/liter of L-methionine, and 1 mM total metal ions with various ratios of iron [from Fe(NH₄)₂(SO₄)₂·6H₂O] to manganese (from MnCl₂·4H₂O). After additional growth for 20 min, the cells were induced with 0.25 mM IPTG and allowed to grow at 30°C for 12 h. AurF was purified as described in ref. 6.

Plasmids pET28a-FdR and pET28a-Fd, which encode a surrogate FdR from *Anabaena* sp. PCC7119 and a surrogate Fd from *Anabaena* sp. PCC7119, respectively, were provided by M. Medina (Universidad de Zaragoza, Zaragoza, Spain) (26). A detailed description of the protein purification protocol may be found in *SI Text*.

EPR. AurF samples were chemically reduced by using equimolar concentration of PMS as redox mediator and various amounts of ascorbate as reducing agent in 20 mM Hepes and 10% glycerol (pH 7.4). Samples were incubated for 30 min in the anaerobic chamber at room temperature. After reduction, samples were placed into quartz EPR tubes (3-mm inner diameter, 4-mm outer diameter) and frozen in liquid nitrogen before EPR measurements. X-band EPR spectra were recorded by using a Varian E-122 X-band spectrometer equipped

with an Air Products Helitran cryostat. EPR measurements were performed at 4 K in 20 mW microwave power, 20 G modulation amplitude, and 8.83 GHz microwave frequency.

Single-Turnover Experiments. For single-turnover experiments, AurF was reduced in equimolar PMS and 4 eq of ascorbate. PMS and ascorbate were removed from the reduced AurF, using a PD-10 desalting column (Amersham Biosciences) and an Amicon Ultra centrifugal filter (Millipore; 10,000 molecular weight cut-off). The reaction of 200 nmol of AurF was started by adding 200 nmol of O₂-saturated pABA solution, and reaction products were identified and quantitated by an Agilent 1100 series HPLC equipped with ZORBAX SB-C18 column. HPLC parameters were as follows: 25°C; solvent A, 1% acetic acid in water; solvent B, methanol; gradient, 10% B for 2 min; then, from 10% B to 100% B over 18 min; flow rate, 0.5 ml/min; and detection by UV absorbance at 268 nm.

Kinetic Studies. Enzyme kinetic assays, using reduced AurF prepared by FdR/Fd, were carried out at 20°C in 1 ml of reaction vials of 20 mM Hepes (pH 7.4). The

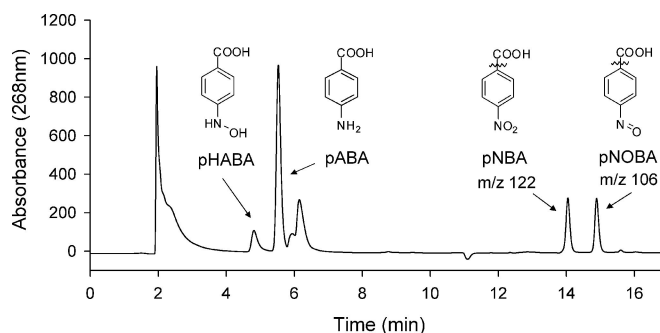


Fig. 6. HPLC analysis of products in the reaction of 0.1 mM AurF, 0.1 mM PMS, 0.2 mM NADH, and 0.5 mM pABA. Products were identified by authentic sample and LC-MS/MS analysis, and the fragmentation patterns are indicated.

assay mixture contained 20 μM FdR, 100 μM Fd, 0.6 μM AurF, 2.5–50 μM pABA, and 750 μM NADPH. Kinetic assays, using reduced AurF prepared by NADH and PMS, were conducted in 75 μM PMS, 0.6 μM AurF, 5–50 μM pABA, and 750 μM NADH in 1 ml of reaction vials of 20 mM Hepes (pH 7.4) at 20°C. All reactions were quenched by rapidly mixing with trifluoroacetic acid to a final concentration of 0.2% and addition of liquid nitrogen, followed by HPLC analysis. The reaction condition designed to trap reaction intermediates included 0.1 mM AurF, 0.1 mM PMS, 0.2 mM NADH, 0.5 mM pABA, and 20 mM Hepes (pH 7.4). The reaction product was analyzed by HPLC coupled to an electrospray ionization (ESI) mass spectrometer (TSQ Quantum; ThermoFinnigan) in a negative-ion mode. The HPLC parameters were identical to those in single-turnover experiments.

Crystallization and Structure Determination. Samples used for crystallization were prepared aerobically from *E. coli* cells harboring the AurF encoding plasmid grown in LB medium. No exogenous metals were added to the growth or purification media. Protein samples prepared in such manner are shown to have an iron to manganese ratio of at least 20:1. After aerobic purification of AurF (in the absence of any exogenous cofactors), samples used for crystallization were further purified by metal affinity, anion exchange, and size exclusion chromatographies. Crystals of AurF could be grown aerobically, using 18–22% polyethylene glycol 8000 and 50 mM Tris-HCl (pH 8.5) as the precipitant. Orthorhombic crystals were grown at 293K over the course of 2 days, and occupy space group $P2_12_12_1$ (two molecules in the asymmetric unit) with unit cell parameters $a = 57.9 \text{ \AA}$, $b = 72.5 \text{ \AA}$, and $c = 138.8 \text{ \AA}$. Monoclinic crystals were grown at 280 K over the course of 4 days and occupy space group $P2_1$ (two molecules in the asymmetric unit) with unit cell parameters $a = 58.4 \text{ \AA}$, $b = 73.3 \text{ \AA}$, $c = 74.7 \text{ \AA}$, and $\beta = 100.9^\circ$. Because crystals in the orthorhombic setting were easier to reproduce, these were used for phasing and structure determination. Anaerobic crystallization was performed by using a Coy glove box apparatus in an inert atmosphere. Before data collection, crystals were transiently soaked in precipitant supplemented with 25% glycerol and directly submerged into liquid nitrogen.

Data from native and heavy-atom soaked orthorhombic crystals of AurF were collected at insertion device beam lines at Argonne National Laboratories. All data were integrated and scaled by using HKL2000 (27). Because of significant nonisomorphism between different crystals, single-wavelength anomalous dispersion methods were pursued for structure determination. A substructure of 10 heavy atom sites was identified from a 2.74 \AA resolution dataset from a mercurial derivative (10 mM ethylmercury bromide, soaked for 24 h). Significant anomalous signal could be observed to 2.85 \AA resolution, and heavy-atom parameter with SHARP, using anisotropic thermal refinement (phasing power = 1.6), yielded an excellent electron density map (figure of merit = 0.407). Phases were extended to 2.74 \AA resolution, using density modification, and model building was initiated by using ARP/wARP (28). Cycles of manual model rebuilding, using XtalView (29), were interspersed with crystallographic refinement, using REFMAC5 (30), until convergence. The final statistics are listed in Table S1. The structures of AurF in the monoclinic setting and the ligand complex were all solved by molecular replacement with PHASER (31), using the coordinates of the orthorhombic form, and refined by using REFMAC5 (30). To confirm the identity of the metal in the crystals, Bijvoet difference Fourier maps were calculated from data collected from a single crystal near the iron ($\lambda = 1.7220 \text{ \AA}$) and manganese ($\lambda = 1.8785 \text{ \AA}$) absorption edges. Figures were generated with either Bobscript (32) or Pymol (33). The coordinates and structure factors have been deposited in the Protein Data Bank (PDB) with ID codes 3CHU (AurF-orthorhombic crystal form), 3CHI (AurF-monoclinic form), and 3CHT (AurF-pNBA complex).

ACKNOWLEDGMENTS. We thank Wilfred van der Donk, Yi Lu, and David Christianson for critical reading of the manuscript; Lisa Keefe and staff at IMCA-CAT (17-ID at Argonne National Labs, APS) and John Chrzas and staff at SER-CAT (22-ID at Argonne National Labs, APS) for facilitating data collection; and Mark Nilges for analyzing EPR data. This work was supported by Office of Naval Research Grant N00014-02-1-0725 (to H.M.Z.) and the National Institute of General Medical Sciences (S.K.N.).

- Winkler R, Hertweck C (2007) Biosynthesis of nitro compounds. *ChemBiochem* 8:973–977.
- Winkler R, Hertweck C (2005) Sequential enzymatic oxidation of aminoarenes to nitroarenes via hydroxylamines. *Angew Chem Int Ed* 44:4083–4087.
- Lee JK, Simurdiak M, Zhao HM (2005) Reconstitution and characterization of aminopyrrolnitrin oxygenase, a Rieske *N*-oxygenase that catalyzes unusual arylamine oxidation. *J Biol Chem* 280:36719–36728.
- He J, Hertweck C (2004) Biosynthetic origin of the rare nitroaryl moiety of the polyketide antibiotic aureothin: Involvement of an unprecedented Ni-oxygenase. *J Amer Chem Soc* 126:3694–3695.
- Lee J, Zhao HM (2006) Mechanistic studies on the conversion of arylamines into aryl nitro compounds by aminopyrrolnitrin oxygenase: Identification of intermediates and kinetic studies. *Angew Chem Int Ed* 45:622–625.
- Simurdiak M, Lee J, Zhao HM (2006) A new class of arylamine oxygenases: Evidence that *p*-aminobenzoate *N*-oxygenase (AurF) is a di-iron enzyme and further mechanistic studies. *ChemBiochem* 7:1169–1172.
- Winkler R, et al. (2007) A binuclear manganese cluster that catalyzes radical-mediated *N*-oxygenation. *Angew Chem Int Ed* 46:8605–8608.
- Winkler R, Richter MEA, Knupfer U, Merten D, Hertweck C (2006) Regio- and chemo-selective enzymatic *N*-oxygenation *in vivo*, *in vitro*, and *in flow*. *Angew Chem Int Ed* 45:8016–8018.
- Zocher G, Winkler R, Hertweck C, Schulz GE (2007) Structure and action of the *N*-oxygenase AurF from *Streptomyces thioluteus*. *J Mol Biol* 373:65–74.
- Krebs C, Matthews ML, Jiang W, Bollinger JM (2007) AurF from *Streptomyces thioluteus* and a possible new family of manganese/iron oxygenases. *Biochemistry* 46:10413–10418.
- Jiang et al. (2007) A manganese(IV)/iron(III) cofactor in *Chlamydia trachomatis* ribonucleotide reductase. *Science* 316:1188–1191.
- Waller BJ, Lipscomb JD (1996) Dioxygen activation by enzymes containing binuclear non-heme iron clusters. *Chem Rev* 96:2625–2657.
- Solomon EI, et al. (2000) Geometric and electronic structure/function correlations in non-heme iron enzymes. *Chem Rev* 100:235–349.
- Fox BG, Froland WA, Dege JE, Lipscomb JD (1989) Methane monooxygenase from *Methylosinus trichosporium* OB3B—Purification and properties of a 3-component system with high specific activity from a type II methanotroph. *J Biol Chem* 264:10023–10033.
- Bollinger JM, et al. (1995) Use of rapid kinetics methods to study the assembly of the diferric-tyrosyl radical cofactor of *E. coli* ribonucleotide reductase. *Methods Enzymol* 258:278–303.
- Hendrich MP, Munck E, Fox BG, Lipscomb JD (1990) Integer-spin EPR studies of the fully reduced methane monooxygenase hydroxylase component. *J Amer Chem Soc* 112:5861–5865.
- Pikus JD, et al. (1996) Recombinant toluene-4-monooxygenase: Catalytic and Mossbauer studies of the purified diiron and Rieske components of a four-protein complex. *Biochemistry* 35:9106–9119.
- Cadieux E, Vrajmasu V, Achim C, Powlowski J, Munck E (2002) Biochemical, Mossbauer, and EPR studies of the diiron cluster of phenol hydroxylase from *Pseudomonas* sp strain CF 600. *Biochemistry* 41:10680–10691.
- Carter P (1971) Spectrophotometric determination of serum iron at submicrogram level with a new reagent (ferrozine). *Anal Biochem* 40:450–458.
- Wang CC, Newton A (1969) Iron transport in *Escherichia coli*: Roles of energy-dependent uptake and 2,3-dihydroxybenzoylserine. *J Bacteriol* 98:1142–1150.
- Silver S, Johnsein P, King K (1970) Manganese active transport in *Escherichia coli*. *J Bacteriol* 104:1299–1306.
- Rosenzweig AC, Frederick CA, Lippard SJ, Nordlund P (1993) Crystal structure of a bacterial non-haem iron hydroxylase that catalyses the biological oxidation of methane. *Nature* 366:537–543.
- Li SY, Wackett LP (1993) Reductive dehalogenation by cytochrome P450(Cam)—substrate-binding and catalysis. *Biochemistry* 32:9355–9361.
- Nordlund P, Sjöberg BM, Eklund H (1990) Three-dimensional structure of the free radical protein of ribonucleotide reductase. *Nature* 345:593–598.
- Lindqvist Y, Huang WJ, Schneider G, Shanklin J (1996) Crystal structure of Δ^9 stearoyl-acyl carrier protein desaturase from castor seed and its relationship to other di-iron proteins. *EMBO J* 15:4081–4092.
- Tejero J, et al. (2003) Involvement of the pyrophosphate and the 2'-phosphate binding regions of ferredoxin-NADP⁺ reductase in coenzyme specificity. *J Biol Chem* 278:49203–49214.
- Otwinowski Z, Minor W (1997) Processing of X-ray diffraction data collected in oscillation mode. *Methods Enzymol* 276:307–326.
- Perrakis A, Morris R, Lamzin VS (1999) Automated protein model building combined with iterative structure refinement. *Nat Struct Biol* 6:458–463.
- McRee DE (1999) XtalView Xfit—A versatile program for manipulating atomic coordinates and electron density. *J Struct Biol* 125:156–165.
- Murshudov GN, Vagin AA, Dodson EJ (1997) Refinement of macromolecular structures by the maximum-likelihood method. *Acta Crystallogr D* 53:240–255.
- McCoy AJ (2007) Solving structures of protein complexes by molecular replacement with PHASER. *Acta Crystallogr D* 63:32–41.
- Esnouf RM (1997) An extensively modified version of MolScript that includes greatly enhanced coloring capabilities. *J Mol Graphics Model* 15:132–134.
- DeLano WL (2002) The PyMOL molecular graphics kernel. (DeLano Scientific, San Carlos, CA).